JCI The Journal of Clinical Investigation

Inhibition of mitophagy drives macrophage activation and anti-bacterial defense during sepsis

Danish Patoli, … , Laurent Lagrost, Charles Thomas

J Clin Invest. 2020. https://doi.org/10.1172/JCI130996.

Research In-Press Preview Inflammation Metabolism

Graphical abstract

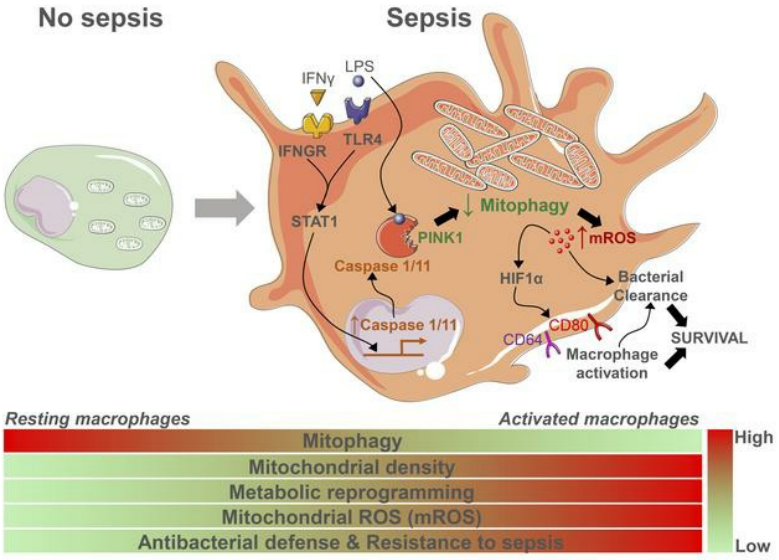

Title: Inhibition of mitophagy drives macrophage activation and anti-bacterial defense during sepsis.

Authors: Danish PATOLI[1,2,‡], Franck MIGNOTTE[1,2,‡,†], Valérie DECKERT[1,2], Alois DUSUEL[1,2], Adélie DUMONT[1,2], Aurélie RIEU[3], Antoine JALIL[1,2], Kevin Van DONGEN[1,2], Thibaut BOURGEOIS[1,2], Thomas GAUTIER[1,2], Charlène MAGNANI[1,2], Naig LE GUERN[1,2], Stéphane MANDARD[1,2], Jean BASTIN[4], Fatima DJOUADI[4], Christine SCHAEFFER[5], Nina GUILLAUMOT[5], Michel NARCE[1,2], Maxime NGUYEN[1,2,6], Julien GUY[7], Auguste DARGENT[1,2,8], Jean-Pierre QUENOT[1,2,8,9], Mickaël RIALLAND[1,2], David MASSON[1,2,10], Johan AUWERX[11], Laurent LAGROST[1,2,10], Charles THOMAS[1,2 *]

Affiliations:

[1]Université de Bourgogne Franche-Comté (UBFC), LNC UMR1231, F-21000 Dijon, France; INSERM, LNC UMR 1231, F-21000 Dijon, France.

[2]LipSTIC LabEx, F-21000 Dijon, France.

[3]Université de Bourgogne Franche-Comté (UBFC), AgroSup Dijon, UMR PAM A 02.102, F-21000 Dijon, France.

[4]Centre de Recherche des Cordeliers, INSERM, Université Sorbonne-Paris-Cité, F-75006 Paris, France.

[5]Université de Strasbourg, CNRS, UMR 7178, LSMBO, F-67000 Strasbourg, France.

[6]Department of Anesthesiology and Intensive Care, University Hospital François Mitterrand, F-21000 Dijon, France

[7]Clinical hematology laboratory, University Hospital François Mitterrand, F-21000 Dijon, France.

[8]Department of Intensive Care, University Hospital François Mitterrand, F-21000 Dijon, France.

[9]Clinical Epidemiology, INSERM CIC 1432 and University of Burgundy, F-21000 Dijon, France

[10]Clinical Biochemistry Department, University Hospital François Mitterrand F-21000 Dijon, France.

[11]Laboratory for Integrative Systems Physiology, Institute of Bioengineering, Ecole Polytechnique Fédérale de Lausanne, CH-1015 Lausanne, Switzerland.

[‡]These authors equally contributed to this work.

[†]We dedicate this work to the memory of Franck Mignotte.

** Correspondence to: Charles THOMAS, phD ; UFR SVTE, Université de Bourgogne, 6 Bd Gabriel, 21000 Dijon, France, Phone : +33 3 80 39 63 19, Email : Charles.Thomas@u-bourgogne.fr*

Abstract.

Mitochondria have emerged as key actors of innate and adaptive immunity. Mitophagy has a pivotal role in cell homeostasis but its contribution to macrophage functions and host defense remains to be delineated. Here we showed that lipopolysaccharide (LPS) in combination with IFNγ, inhibits PINK1-dependent mitophagy in macrophages through a STAT1-dependent activation of the inflammatory caspases 1 and 11. In addition, we demonstrated that the inhibition of mitophagy triggers classical macrophage activation in a mitochondrial ROS-dependent manner. In a murine model of polymicrobial infection (cecal ligature and puncture), adoptive transfer of *Pink1*-deficient bone marrow or pharmacological inhibition of mitophagy promoted macrophage activation which favored bactericidal clearance and lead to a better survival. Reciprocally, mitochondrial uncouplers, that promote mitophagy, reverse LPS/IFNγ-mediated activation of macrophages and lead to immuno-paralysis with impaired bacterial clearance and lowered survival. In critically ill patients, we showed that mitophagy is inhibited in blood monocytes of patients with sepsis as compared to non-septic patients. Overall, this work demonstrates that the inhibition of mitophagy is a physiological mechanism that contributes to the activation of myeloid cells and improves the outcome of sepsis.

Introduction.

Sepsis is one of the leading causes of morbidity and mortality in intensive care units (1). Strategies that blunt the inflammatory responses have failed to improve survival, whereas those that enhance host defenses have recently gained more attention (2, 3). Myeloid cells have a crucial role in the clearance of pathogens. After an initial inflammatory phase, classically activated macrophages (M1) undergo reprogramming to an alternate M2 phenotype (4). This second phase contributes to secondary immune suppression, known as immuno-paralysis, that occurs during sepsis and which counteracts the removal of infectious agents to ultimately worsen pathological conditions (5). The pivotal role of mitochondria in immune cells and immunity is now widely appreciated (6-8). In rodent models of sepsis, alterations of mitochondrial function have been described in the heart, the muscle or the liver (9-11). Reduced activity of the mitochondrial respiratory chain has also been demonstrated in blood leukocytes of septic patients (12). These mitochondrial dysfunctions have been proposed to trigger the activation of the NLRP3 inflammasome in macrophage leading to the release of the IL-1β, in particular through mitochondrial reactive oxygen species (mROS) (13-15).

More broadly, alterations of mitochondria have a prominent role in multi-organ failure in septic patients (16). Mitochondrial quality is tightly linked to mitophagy and mitochondrial dynamics. Classically, defective mitochondria have decreased mitochondrial membrane potential and enhanced fission. This leads to the stabilization and accumulation of PINK1 on the outer mitochondrial membrane (OMM), which activates the E3 ubiquitin-ligase Parkin and leads to its recruitment onto mitochondria. Parkin then decorates mitochondria with ubiquitin chains, which are sequentially phosphorylated by PINK1. The accumulation of phospho-ubiquitin chains on the OMM triggers the recruitment of the autophagy receptors and commits damaged mitochondria to mitophagy (17, 18). In rodent models of sepsis, prolonged impairment of mitophagy due to the ablation of *Pink1* or *Parkin* genes results in reduced survival (13, 19). By contrast, adoptive transfer of bone marrow deficient in *Dj-1*, a PINK1 and Parkin partner (20, 21), protects the

recipient-mice against sepsis (22). Therefore, the role of mitophagy in immune cells and host defense remains to be clarified.

Mitochondrial function and mitophagy are linked to mROS production (14, 23). ROS signaling and oxidative stress have a pivotal role in septic conditions (23, 24). LPS-induced nitric oxide production, which inhibits complex I, complex III and complex IV of the electron transport chain (ETC), is thought to promote mROS production (7). In activated macrophages, oxidation of succinate at complex II (CII) significantly augments mROS production. This results in the stabilization and activation of Hypoxia Inducible Factor 1 α (HIF1α) and the subsequent release of IL-1β (8). LPS-mediated increase in CII activity was also shown to contribute to pathogen clearance (25). Additionally, activation of Toll-like Receptors (TLR) 1-2-4 signaling increases mROS production through TRAF6-dependent destabilization of the complex I. mROS was proposed to directly contribute to macrophage bactericidal activity (26, 27). Interestingly, the inhibition of mitophagy has been described as a major source of mROS (14). So far, investigations in mouse models deficient for mitophagy argue in favor of a deleterious role of the inhibition of mitophagy in the outcome of sepsis. Here, we investigated the role of mitophagy in macrophage activation through in vitro and in vivo approaches and assessed the consequences of its modulation in mouse models of sepsis and in critically ill patients.

Results.

LPS enhances mitochondrial ROS production through the inhibition of mitophagy in macrophages.

Enhanced production of mROS in macrophages has been proposed to result from the activation of TLR 1-2-4 signaling (26). We also noticed an increase in mROS with Pam2CSK4 (TLR2-6 agonist), Poly(I:C) (TLR3 agonist), and R848 (TLR7-8 agonist) (Figure 1A). The quantification of mitochondrial density with mitotracker green FM (a mitochondrial dye insensitive to $\Delta\psi_m$) by flow cytometry revealed that increased mitochondrial density was a specific signature of the exposure to LPS (a component of gram-negative bacteria), relative to mROS production that was similarly induced by different TLR agonists (Figure 1A). An increase in mitochondrial density was also observed with live gram-negative bacteria (*E. coli* O55:B5), but not with the gram-positive bacterial strain *B. subtilis* (Figure S1A). This raises the possibility that the activation of TLR4 signaling promotes mROS production through a mechanism distinct from other TLRs. The inhibition of mitophagy is a major source of mROS (14). Similar to LPS-treated raw 264.7 macrophages, raw 264.7 macrophages exposed to pharmacological inhibitors of mitophagy (Mdivi-1, 3-Methyladenine (3-MA), Apigenin and 4,5,6,7-Tetrabromobenzotriazole (TBB) (see supplementary information)) displayed a concomitant increase in mROS production and mitochondrial density (Figure1B and FigureS1B-C). This rise in mROS production and mitochondrial density induced by LPS was markedly enhanced by IFNγ co-treatment, and thus appeared as a feature of classically activated macrophages (Figure 1C). This early raise in mitochondrial density was also observed by flow cytometry and microscopy in activated raw 264.7 macrophages transfected with an expression vector, coding for LSSmOrange-cytochrome C oxidase subunit VIII (MitoOrange) (Figure S1D).

The fast time-course of LPS- and LPS/IFNγ-mediated increase in mitochondrial density in macrophages, associated with enhanced mROS production (Figure1D and S1A), suggests that this event stems from an inhibition of mitophagy rather than from mitochondrial biogenesis which

occurs slower (28). We hence measured the spectral shift of mitochondrial-targeted mKeima (mt-mKeima) by flow cytometry, which specifically monitors autophagosomal engulfment of mitochondria (see supplementary information). Exposure of raw 264.7 macrophages to LPS/IFNγ for 6h or 18h, resulted in an increased signal corresponding to the excitation at neutral pH (no mitophagy) whereas the signal from mt-mKeima at acidic pH (mitophagy) was reduced. Consequently, the pH4 to pH7 ratio of mt-mKeima was reduced upon LPS/IFNγ exposure (Figure 1E, upper panel), indicating a marked reduction in mitophagy in activated macrophages. By contrast, as previously reported in the literature, quantification of autophagic vacuoles using cyto-ID (Figure 1E, lower panel) confirmed that LPS/IFNγ treatment induces autophagy in a time-dependent manner. LPS-induced autophagy has been shown to play an important role in macrophage activation and phagocytosis (29). Our data suggest that, although overall autophagy is increased, organelle-targeted autophagy processes, such as mitophagy, do not follow a similar trend. To further confirm our observations, we also assessed the protein levels of several mitophagy (PINK1, Parkin, DJ-1) and mitochondrial fission (DRP-1) markers, which were all reduced in a time-dependent manner in Bone marrow-derived macrophages (BMDMs) (Figure 1F), as well as in raw 264.7 (Figure S1E). Reduced levels of Parkin, PINK1 and their partner DJ-1 (Park7) have been linked to defective mitophagy and autosomal recessive forms of Parkinson's disease (30).

Inhibition of mitophagy is a feature of activated macrophages.

Stat1-deficient macrophages failed to commit to classical activation as confirmed in vivo in LPS-injected Stat1-deficient mice (Figure S2A) and in vitro in Stat1-deficient BMDMs and raw 264.7 macrophages (Figure S2B-C). Noticeably, CD64 and CD80 M1 polarization markers were unresponsive to LPS in Stat1-deficient BMDMs and in STAT1 siRNA transfected raw 264.7 macrophages (Figure S2B-C). Along with this, LPS-mediated inhibition of mitophagy was absent in Stat1-deficient BMDMs and raw 264.7 macrophages as indicated by the normalization of the

protein levels of mitophagy markers (Figure 1F and S1E). These data highlight the inhibition of mitophagy as a feature of activated macrophages.

Mitochondrial uncouplers are classically used to promote mitophagy (18, 28). As expected, exposure of raw 264.7 macrophages to 2,4-dinitrophenol (2,4-DNP) or carbonyl cyanide m-chlorophenyl hydrazone (CCCP) promoted mitophagy and increased PINK1, DJ-1 and DRP1 protein levels (Figure 1G and S1F). 2,4-DNP and CCCP treatment reversed LPS/IFNγ-mediated inhibition of mitophagy as indicated by the normalization of PINK1, Parkin, DJ-1 and DRP1 levels (Figure 1G and S1F). The recruitment of Parkin onto mitochondria is also a key determinant of the commitment of mitochondria to mitophagy. In most cell types, at steady state, PINK1 and Parkin are indiscernible in mitochondria. Here, in quiescent mouse peritoneal macrophages, we observed a co-localization of PINK1 and Tom20 (an OMM marker) on round-shaped mitochondria (Figure 2A). Parkin was also detected on isolated mitochondria in raw 264.7 macrophages (Figure S3A). This argues in favor of a high basal mitophagy flux in quiescent macrophages. The mitochondrial localization of PINK1 and the recruitment of Parkin onto mitochondria were, however, dampened upon LPS/IFNγ-mediated macrophage activation (Figure 2A and Figure S3A).

LPS/IFNγ-dependent activation of macrophages is associated with high mitochondrial membrane potential and fused mitochondria.

Mitophagy fluxes are intimately linked to alteration in mitochondrial dynamics as well as cell bioenergetics. Whereas the induction of mitophagy is associated with an increase in mitochondrial fission and a drop in Δψm, enhancement of mitochondrial fusion and high Δψm are observed concomitantly with the inhibition of mitophagy (31). In line with this, raw 264.7 macrophages and peritoneal macrophages treated with LPS/IFNγ for 6h, displayed a marked reconfiguration of the mitochondrial network, which became fused, denser and more connected (Figure 2A and Figure S3B). JC-1 dye allows visualizing mitochondria with both low (JC-1 monomers, green) and high Δψm (JC-1 aggregates, red) (Figure 2B). Image binarization of JC-1-stained macrophages

confirmed the robust increase in the mitochondrial network in LPS/IFNγ-treated macrophages, as soon as 6h (Figure 2B).

Whereas, mainly low Δψm mitochondria were observed in quiescent macrophages, the proportion of high Δψm mitochondria (JC-1 aggregates) rapidly increased after the exposure to LPS/IFNγ (Figure 2B). The time-dependent increase in Δψm upon macrophage activation was confirmed by flow cytometry in raw 264.7 macrophages (Figure 2C). Interestingly, JC-1 monomers were also markedly increased, further confirming that LPS/IFNγ increases the mitochondrial density in macrophages; and this, with a strong representation of high-Δψm mitochondria as shown by the concomitant increase in JC-1 aggregates (Figure 2C). The enhancement of Δψm in activated macrophages was confirmed by TMRM staining (Figure 2F).

Inhibition of mitophagy contributes to the survival of activated macrophages.

Within the same timeframe, oxygen consumption rate (OCR) was reduced in BMDMs exposed to LPS/IFNγ for 6h whereas extracellular acidification rate (ECAR) was enhanced (Figure 2D-E). This specificity of LPS-mediated metabolic rewiring in myeloid cells as compared to other TLRs agonists was also reported by others (32). This metabolic feature that was maintained 24h after exposure to LPS/IFNγ (not shown) underlies the metabolic rewiring of LPS-activated macrophages towards glycolysis (6, 7). Noteworthy, the OCR and ECAR profiles of BMDMs exposed the mitophagy inhibitor mdivi-1 were similar to those of classically activated macrophages (Figure 2D-E). Despite the strong reduction of OCR and the increase in ECAR, exposure to LPS/IFNγ did not increase cell death (Figure 2G). The survival LPS/IFNγ-exposed macrophages could be explained by mitochondrial fusion (33, 34). By contrast, the stimulation of mitophagy with 2,4-DNP in activated raw 264.7 macrophages enhances cell death. Therefore, inhibition of mitophagy may also contribute to cell survival in conditions of low respiration.

LPS triggers the inhibition of mitophagy in myeloid cells in vivo.

Gram-negative bacteria are the predominant species in the caecal ligation and puncture (CLP) model of polymicrobial infection (35), which we used to explore the translational relevance of our

in vitro findings. Female C57BL6/J mice underwent CLP- or sham-surgery. Mitophagy was assessed extemporaneously on freshly collected blood peritoneal leukocytes through the measurement of mitochondrial density by flow cytometry. Samples were collected after CLP- or sham-surgery at indicated time points (Figure 3, Figure S4). Blood and peritoneal leukocytes were incubated for 10 min with mitotracker green FM before immunostaining and then processed for flow cytometry analysis. In the blood, the proportion of monocytes ($CD45^{+}$ $CD115^{+}$) and inflammatory monocyte subpopulation ($CD45^{+}$ $CD115^{+}$ $CD11b^{Hi}$ $Ly6C^{Hi}$) were not significantly affected by polymicrobial infection except 24h post CLP for inflammatory monocytes (Figure S4C and S4D). By contrast, monocytes and the subpopulation of inflammatory monocytes showed both a marked increase in mitochondrial density at 2h and 24h post-infection (Figure 3A and 3B). We also observed a robust increase in mitochondrial density in peritoneal macrophages at early time points (2h, 6h) after CLP surgery compared to sham surgery (Figure 3C). These changes were independent to the proportion of peritoneal macrophages (Figure S4E).

$CD64^{Hi}$ $Mitotracker^{Hi}$ macrophage subpopulation is highly increased during sepsis.

As expected, peritoneal macrophages from infected mice displayed a significant rise in the levels of the macrophage activation markers CD64 (FcγRI) and CD80 (Figure S4F-G). CD64 level in myeloid cells has been positively correlated to the severity of sepsis (36). Accordingly, the increase in CD64 level in peritoneal macrophages of CLP-operated mice was more pronounced as compared to CD80 (Figure S4G). We identified a subpopulation of $CD64^{Hi}$ macrophages with a high mitochondrial density ($CD64^{Hi}$ $Mitrotracker^{Hi}$) whose proportion was time-dependently increased in macrophages from CLP-operated animals (Figure 3D). In non-infected animals, although the proportion of peritoneal $CD64^{Hi}$ macrophages was extremely low, mitochondrial density was significantly higher than in $CD64^{Lo}$ or $CD80^{Lo}$ and $CD80^{Hi}$ macrophages (Figure S4H-I). To confirm that the phenotype of monocytes and macrophages observed after CLP-surgery was due to LPS produced by gram-negative bacteria, we assessed the impact of low (0.5mg/kg) and high (15mg/kg) doses of intraperitoneally injected LPS. Both doses lead to a similar

phenotype with an increase in mitochondrial density in peritoneal macrophages and blood monocytes, as well as a rise in CD64^{Hi} Mitrotracker^{Hi} macrophages subpopulation as soon as 1h exposure (Figure S4J-L).

LPS mediates the inhibition of mitophagy in a STAT1-dependent manner.

Stat1-deficient mice are defective with regards to the activation of macrophages (Figure S2A-C). This phenotype was associated with an absence of reduction of the protein levels of mitophagy and mitochondrial fission checkpoints (Figure 1F and Figure S1E). We further explored the impact of STAT1 invalidation on mitophagy and showed that Stat1-deficient mice also fail to show a CLP- and LPS-mediated increase in mitochondrial density at 2h in both CD64^{Hi} peritoneal macrophages and blood monocytes (Figure 4A and 4B). These observations were confirmed in vitro in BMDMs and raw 264.7 macrophages (Figure 4C and 4D). Additionally, changes in mROS production, Δψm and respiration associated with LPS/IFNγ–mediated inhibition of mitophagy were reduced or normalized in Stat1-deficient BMDMs (Figure 4E-G).

STAT1 inhibits mitophagy through inflammatory caspases 1 and 11

We then explored whether the above phenomenon was related to the inability of Stat1-deficient macrophages to commit to classical activation or to a STAT1-dependent modulation of mitophagy. Caspase 1 was shown to inhibit mitophagy by cleaving and inactivating Parkin subsequently to its translocation to mitochondria (37, 38). Interestingly, IFNγ was shown to regulate *caspase 1* levels and activity (39). We showed here that STAT1-mediated LPS/IFNγ-dependent regulation of *caspase 1* at mRNA and protein levels in BMDMs did not affect NLRP3 levels (Figure 5A-B). A similar pattern of regulation was observed for *caspase 11* in raw 264.7 macrophages (Figure S5A-B), another key inflammatory caspase regulated and activated by LPS, which controls interleukin 1β (IL-1β) secretion by potentiating caspase 1 activation (40). STAT1-dependent regulation of *caspase 11* was only assessed in raw 264.7 macrophages since Stat1-deficient mice are on a 129SV genetic background and do not express caspase 11 (41). Similarly to caspase 1 (37), the exposure of raw 264.7 macrophages to LPS/IFNγ leads to the mitochondrial translocation of

caspase 11 (Figure S5C). The inhibition of caspases with zVAD-FMK (Figure 5C), as well as RNAi-mediated gene silencing of *caspase 1* or *caspase 11* resulted in the abrogation of LPS/IFNγ-mediated drop in PINK1 protein levels in raw 264.7 macrophages (Figure S5D). This translates into a less pronounced increase in mitochondrial density in activated macrophages exposed to zVAD-FMK or caspase 1 or 11 siRNA (Figure 5D and S5E). Surprisingly, LPS/IFNγ-mediated Parkin down-regulation was more pronounced upon *caspase 1* or *caspase 11* gene silencing (Figure S5D). This observation suggests that PINK1 plays a central role in LPS/IFNγ-mediated inhibition of mitophagy in macrophages.

The inflammatory caspases 1 and 11 degrade PINK1.

Caspase 11 was shown to degrade TRPC1 (42); caspase 1 is endowed with similar proteolytic properties. Therefore, we speculated that caspase 1 and 11 could impact on mitophagy by degrading PINK1. PINK1 has a pivotal role in mitochondrial quality control and is evolutionary conserved (43). Using Cascleavage 2.0, Prosper 2.0 and CasDB, several conserved caspase cleavage sequences were identified in human, mouse and *Tribolium castaneum* PINK1 (T. cast. PINK1). Recombinant *Tribolium castaneum* PINK1 that retains its kinase activity as compared to human and mouse PINK1 (43-45) was used for further in vitro experiments. This active recombinant PINK1 was incubated with active recombinant human caspase 1 or 4 (the human orthologue of caspase 11) in the presence or absence of zVAD-FMK or LPS. Protein levels were assessed using polyacrylamide gels containing 2,2,2-Trichloroethanol (TCE), which allows fluorescent detection of proteins after UV exposure. Both recombinant caspase 1 and 4/11 led to reduced PINK1 levels (Figure 5E and S5F). In agreement with LPS-binding capacity of caspase 4/11 (46, 47), the reduction of PINK1 was more pronounced when caspase 4 was incubated with LPS (Figure S5F). Unexpectedly, a similar observation was made for caspase 1 (Figure 5E and S5F). Beyond 1h incubation with recombinant caspase 4, *Tribolium castaneum* PINK1 was not anymore detectable (not shown). Oppositely to LPS, zVAD-FMK treatment reduced caspase-mediated PINK1 degradation (Figure 5E and S5F).

LPS/IFNγ-mediated inhibition of mitophagy triggers classical activation of macrophages through mitochondrial ROS.

The inhibition of mitophagy is a critical source of mROS (14) (Figure 1B and S1B). Since we showed that the inhibition of mitophagy is an early feature of macrophage activation, we examined whether mROS could directly trigger the classical activation of macrophages. Mitochondrial CI and CIII, whose activities were reduced in LPS/IFNγ-exposed raw 264.7 macrophages (Figure S6A), are two major sources of mROS (14, 48). We thus used rotenone and antimycin A, respective CI and CIII inhibitors, to promote mROS production (Figure S6B) (14). However, only CIII inhibition efficiently promoted an increase in macrophage activation markers in raw 264.7 (Figure 6A and S6C). This parallels the increase in mROS, which was more pronounced with antimycin A, compared to rotenone (Figure S6B). Along with raw 264.7 macrophage activation, antimycin A triggered the release of inflammatory cytokines (Figure S6E). The exposure of BMDMs to MitoParaquat, a mROS generator, further strengthens the role of mROS in macrophage activation (Figure S6D). Moreover, scavenging of mROS induced by LPS/IFNγ with mitoTEMPOL, a mROS scavenger, or with N-acetyl-L-cystein (NAC), a general ROS scavenger, decreased raw 264.7 macrophage activation (Figure 6B and S6F). Accordingly, ROS scavengers also prevented LPS/IFNγ-mediated inflammatory cytokines release as well as phagocytosis of latex beads in raw 264.7 macrophages (Figure S6G-H).

Inhibition of mitophagy induces the classical activation of macrophages through HIFα.

Hypoxia-inducible Factor 1α (HIF1α) contributes to the functional reprogramming of monocytes during sepsis (49) and to the metabolic reprogramming during macrophage activation where it can be activated and stabilized by succinate or mROS (48, 50, 51). Accordingly, HIF-1α protein levels were increased by both LPS/IFNγ and mdivi-1 exposure in raw 264.7 macrophages (Figure S6K). Interestingly, echinomycin, a pharmacological inhibitor of HIF1α (52), blunted the activation of raw 264.7 macrophages triggered by LPS/IFNγ, antimycin A, MitoParaquat and mdivi-1 (Figure 6C, S6D and S6I-J). In agreement with the contribution of mROS to macrophage activation, we

showed that mdivi-1 as well as other mitophagy inhibitors promoted classical activation of raw 264.7 macrophages as assessed by flow cytometry or by gene expression (Figure 6D-E, Figure S7A-B). The inhibition of mitophagy in raw 264.7 macrophages went also along with elevated inflammatory cytokine release and increased phagocytosis of latex beads (Figure S7C-D). In line with their ability to commit raw 264.7 macrophages toward an inflammatory phenotype, pharmacological inhibitors of mitophagy boosted their bactericidal activity (Figure 6F and S7E). Oppositely to mdivi-1, exposure of activated raw 264.7 macrophages to the mitochondrial uncouplers CCCP and 2,4-DNP promotes mitophagy and reverses LPS/IFNγ-mediated inhibition of mitophagy (Figure 1g and S1f). This translates into a reduction of raw 264.7 macrophage activation as well as bactericidal activity (Figure 6G-I and S7F-G).

Inhibition of mitophagy in myeloid cells protects against bacterial infection.

We were able to translate our results in vivo in mice since the administration of mitochondrial uncouplers alone or in combination with LPS in mice mirrored our in vitro observations. The induction of mitophagy was associated with reduced mitochondrial density in peritoneal macrophages. More strikingly, LPS-mediated inhibition of mitophagy in peritoneal macrophages was reversed by CCCP and 2,4-DNP administration (Figure S8A-B). Then, we used a single intraperitoneal injection of 2,4-DNP (10mg/kg) to promote mitophagy 24h prior to CLP surgery. Whereas 2,4-DNP did not impact on the survival of sham-operated animals, it significantly reduced the survival of CLP-operated animals (Figure 7A). As expected, the mitochondrial density of peritoneal macrophages was reduced as a consequence of 2,4-DNP-induced mitophagy (Figure S8C). This stimulation of mitophagy translated into a decrease in macrophage activation as illustrated by the reduction of the proportion of $CD80^{Hi}CD64^{Hi}$ macrophages and lowered levels of plasma inflammatory cytokines (Figure 7B, S8D and S8G). The total number of peritoneal macrophages was not altered by 2,4-DNP (Figure S8E). This dampened macrophage activation resulted in a higher bacterial load in the peritoneal cavity of 2,4-DNP-injected animals (Figure 7C), with a similar trend in the liver (Figure S8F). No changes in blood bacteremia were observed (not

shown). We ranked peritoneal bacterial load above 1.10^6CFU/mL as high bacterial load and noticed that animals with the highest bacterial load presented a significant reduction in the proportion of CD64^{Hi} Mitotracker^{Hi} macrophages in the peritoneal cavity (Figure S8H).

Early inhibition of mitophagy in myeloid cells is predictive factors of survival upon sepsis.

This led us to assume that the inhibition of mitophagy is protective against bacterial invasion during sepsis. In line with this, we found a significant positive correlation between mitochondrial density in Ly6C^{Hi} blood monocytes collected 2h after CLP surgery and the survival of animals over a period of 10 days (Figure 7D). More expectedly, the percentage of Ly6C^{Hi} blood monocytes at 2h was also correlated with mouse survival (Figure S8J) but the percentage of Ly6C^{Hi} blood monocytes and mitochondrial density in these monocytes were not correlated (Figure S8K). Therefore, mitochondrial density in Ly6C^{Hi} blood monocytes at early time point after polymicrobial infection is an independent predictor of survival. Finally, we sorted animals into short-term (<72h survival) and long-term (>72h survival) survivors and showed that relative to short-term survivors, long-term survivors had higher mitochondrial density (mitophagy inhibition) in Ly6C^{Hi} blood monocytes (Figure S8I).

Inhibition of mitophagy in myeloid reduces bacterial load upon sepsis.

To further confirm, the protective role of mitophagy inhibition in myeloid cells against polymicrobial infection, we injected C57BL6/J mice intraperitoneally with mdivi-1 (50mg/kg) 24h prior to sham- or CLP-surgery. The intraperitoneal injection of mdivi-1 in mice mimicked the increase in the proportion of CD64^{Hi} Mitotracker^{Hi} peritoneal macrophages observed in CLP-operated or LPS-injected mice (Figure S9A). Moreover, in accordance with the inhibition of mitophagy promoted by mdivi-1, the mitochondrial density was also increased in Ly6C^{Hi} blood monocytes (Figure S9B). Oppositely to 2,4-DNP-induced mitophagy, the intraperitoneal injection of mdivi-1, 24h prior to CLP surgery, leads to a significant increase in the survival of mdivi-1-treated mice (Figure 7E). The increased proportion of activated macrophages in the peritoneal cavity (Figure 7F) contributes to the reduced bacterial load observed in the peritoneal cavity

(Figure 7G), the liver and the blood of mdivi-1-injected mice (Figure S9C-D) and their improved survival as compared to vehicle-treated mice. Noteworthy, the proportion of $CD64^{Hi}$ $Mitotracker^{Hi}$ peritoneal macrophages also higher in mdivi-1-treated mice that underwent CLP surgery (Figure S9E) whereas the percentage of total peritoneal macrophages was not affected by mdivi-1 pre-treatment (Figure S9F). Since our in vitro data argue in favor of a key role of PINK1-dependent mitophagy in the LPS-dependent activation of myeloid cells, we performed transplantation of *Pink1*$^{+/+}$ or *Pink1*$^{-/-}$ bone marrow in C57BL6/J recipient mice (BMT *Pink1*$^{+/+}$, BMT *Pink1*$^{-/-}$). After 5 weeks of recovery, chimeric mice with *Pink1*-hematopoietic deficiency and their control that received $PINK^{+/+}$ bone marrow underwent CLP surgery (Figure 7H). Similarly, to the pharmacological inhibition of mitophagy, hematopoietic deficiency in *Pink1* leads to an increase in mitochondrial density in peritoneal macrophages (Figure S9G). More spectacularly, survival post CLP was improved in mice transplanted with *Pink1*$^{-/-}$ bone marrow (Figure 7H). This can be attributed, at least in part, to the increased proportion of activated macrophages (Figure 7I) and of $CD64^{Hi}$/$Mitotracker^{Hi}$ macrophages (Figure S9H) in the peritoneal cavity which contribute to a lower bacterial load in the peritoneal cavity (Figure 7J) and in the liver (Figure S9I). Noteworthy, the percentage of peritoneal macrophages did not differ between *Pink1*$^{-/-}$ and *Pink1*$^{+/+}$ chimeric mice (Figure S9J).

Inhibition of mitophagy in blood monocytes is a marker of sepsis in critically ill patients.

Finally, we aimed to assess the clinical relevance of our in vitro and in vivo findings in mice. Mitochondrial density was assessed in blood monocytes of thirty-two critically ill patients within 8h after their admission in intensive care unit (ICU). Blood markers of inflammation, metabolism, liver function, renal function, cardiac function, hemodynamics and tissue perfusion monitored within the same timeframe were collected from the medical records. The causes of admission as well as age and gender distribution of patients are depicted in table S1 (median of age, 59.5y/o (non-septic patients) *vs* 62y/o (septic patients), ns, p=0.55). Sixteen patients were presenting sepsis according to the definition of the Sepsis-3 task force (53). Mitochondrial density in blood

monocytes was significantly higher in septic patients as compared to non-septic patients (Figure 8A). A similar observation was made in classical and non-classical monocytes sub-populations (Figure S10B). Of note, the percentage of monocytes was not significantly different between the two groups of patients despite a trend to be lower in septic patients (median: 9.2% (non-septic) vs 4.8% (septic)) (Figure S10C). The percentage of classical monocytes ($CD14^{++}CD16^{-}$) was significantly reduced in septic patients (median: 83.7% of total monocytes (non-septic) vs 68.9% (septic)) (Figure S10C). Non-classical (inflammatory) monocytes as well as intermediate monocytes displayed a non-significant trend toward an increase (Figure S10C).

Inflammatory markers, namely C-reactive protein (CRP) and procalcitonin (PCT), have a pivotal role in the diagnosis of sepsis. Both were above the normal range in all ICU patients and, as expected, with significantly higher levels in septic patients (Figure 8B). PCT, as a marker of severe infection, was particularly increased in septic patients with a median 10-fold higher median value as compared to non-septic patients (Figure 8B). Other inflammatory markers such as leukocytes count and neutrophil count were not significantly different between the two groups (Figure S10D). Lactate levels are an indicator of tissue perfusion used as criteria of septic shock in patient with sepsis (53). Here, blood lactate levels did not allow to differentiate both groups of patients (Figure 8B). The median of blood markers of renal function (Figure S10E), metabolism (Figure S10F), liver function (Figure S10G), coagulation (Figure S10H), cardiac function (Figure S10I), tissue oxygenation and hemodynamics (Figure S10J) were almost all out of the normal range (normal range of healthy patients are presented in bold italic enclosed in square brackets) for both group of critically ill patients. With the exception of arterial pH, none of the recorded parameters allowed to discriminate between septic and non-septic patients. Therefore, mitochondrial density in monocytes arose as a potential biomarker of sepsis in critically ill patients similarly to CRP and PCT. Because of high variation among patients, we also analyzed the correlation between all these monitored parameters (Figure 8C). Only few parameters were significantly correlated. As expected, CRP and PCT were highly correlated (spearman r=0.82,

p=0.0003) (Figure 8C). Interestingly, similarly to PCT, mitochondrial density in total monocytes (spearman r=0.56, p=0.01), as well as classical (spearman r=0.59, p=0.006) and inflammatory monocytes (spearman r=0.54, p=0.01), were positively correlated to CRP (Figure 8C). These data further suggest that mitophagy levels in blood monocytes could be a useful marker for sepsis in critically ill patients. Further studies are required to assess whether this parameter is differentially altered according to sepsis severity or survival.

Discussion

Altogether our observations showed that the early inhibition of mitophagy in myeloid cells contributes to their activation and improves the outcome of gram-negative bacterial infections and septic conditions in mice. The translational value of these findings was documented and mitophagy level in blood monocytes was highlighted as a biomarker of sepsis in critically ill patients

The current view is that the induction of mitophagy protects against sepsis, based on the observation that altered mitochondrial function leads to an excessive mROS production, the release of mtDNA and to the activation of the NLRP3 inflammasome (14, 15, 54). Nevertheless, the contribution of mROS to sepsis is controversial. mROS lead to NLRP3 activation which is associated with IL-1β release and reduced survival (14, 40). However, in macrophages, mROS production contributes to bacterial clearance and host defense (26, 27). In addition, mROS scavenging with SkQ1 or MitoTEMPOL in CLP-mediated polymicrobial infection in mice significantly reduced survival (55). Our data demonstrating that LPS/IFNγ-mediated inhibition of mitophagy in macrophages leads to enhanced mROS production and triggers the activation of macrophage are in line with these observations.

Classically, mitophagy is assessed by western blotting and microscopy. Such strategies are not easily applicable to macrophages in vivo at early time points following bacterial infection. To overcome this technical issue, we first showed that the assessment of mitochondrial density by flow cytometry is a reliable marker of mitophagy. Then, we transposed this approach to freshly collected blood and peritoneal fluid in mice and critically ill patients. This cytometry approach allowed us to track mitophagy extemporaneously in subsets of immune cells extemporaneously as soon as 1h post-infection. While our study focused on early time points, most of previous studies that investigated mitophagy in the context of sepsis considered time points beyond 24h. Earlier reports described an induction of mitophagy during sepsis (13, 56, 57). Our data do not

oppose such previous studies but rather bridge a gap by focusing at early stages of macrophage activation. In vitro, we observed that LPS/IFNγ-exposed BMDMs displayed a drop in the protein levels of mitophagy checkpoints. After this initial decrease, we noticed an increase in PINK1, Parkin and DRP1 protein levels in BMDMS exposed to LPS/IFNγ over 18h (not shown). Therefore, after an initial decrease upon macrophage activation, mitophagy is re-activated in response to the deleterious impact of a perpetuated inhibition of mitophagy.

Our study also portrays the metabolic shifts associated with macrophage activation and LPS/IFNγ-mediated inhibition of mitophagy. A drop in the Δψm is a well-characterized trigger that initiates PINK1-dependent mitophagy (17, 31). In line with this, we found that LPS/IFNγ-mediated inhibition of mitophagy in macrophages is linked to a rise in Δψm with hyperfused mitochondria. Classically, such a phenotype is related to enhanced OXPHOS (6, 58). Nevertheless, in LPS/IFNγ-activated macrophages mitochondrial respiration drops, whereas extracellular acidification increases. This underlies their glycolytic shift (6-8). Of note, this metabolic profile is a feature LPS/IFNγ-activated macrophages as the activation state triggered by the TLR2 ligand Pam3CysSK4 is associated with a different metabolic signature characterized by an increased extracellular acidification rate along with an increased oxygen consumption (32). Interestingly, by inhibiting mitophagy with mdivi-1, we observed a metabolic rewiring similar to this observed in LPS/IFNγ-activated macrophages. Similarly, *Pink1*-deficiency is associated to a fall in mitochondrial respiration, a reduction in CI, CIII and CIV activity and a metabolic reprogramming towards glycolysis (59, 60). Along with these changes, *Pink1*-deficient myocytes exhibit a pronounced increase in Δψm compared to wild-type myocytes (61) which further consolidates the idea that mitophagy inhibition contributes to the metabolic rewiring associated to macrophage activation. In *Pink1*-deficient mouse embryonic fibroblasts, the maintenance of cell viability involves HIF-1α subsequently to its activation by mROS (60). In our settings, we showed that mROS and HIF-1α also have a pivotal role in macrophage activation following LPS/IFNγ-mediated

mitophagy inhibition.

Whereas mROS can be generated by the activation of various TLR agonists (26), we showed that upon macrophage activation mROS generated in a mitophagy-dependent manner are exclusively triggered by LPS. In addition to TLR4, STAT1 signaling holds a central position in LPS/IFNγ-mediated macrophage activation (4, 62). We demonstrated that STAT1 is directly involved in LPS/IFNγ-mediated inhibition of mitophagy. Interestingly, a link between STAT1 and mitochondrial function was previously suggested (63-65). Our work also showed that the activation of STAT1 signaling results in the inhibition of mitophagy in a caspase 1- and caspase 11-dependent manner. These interconnected inflammatory caspases are involved in LPS-dependent activation of the NLRP3 inflammasome, pyroptosis and IL-1β release (40, 66). Upon activation of the NLRP3 inflammasome, caspase 1 was shown to translocate to mitochondria to block mitophagy by degrading Parkin (37, 38). Here we showed that the pan-caspase inhibitor z-VAD or siRNA targeting caspase 1 abrogate LPS/IFNγ-mediated down-regulation of PINK1 protein levels and subsequently inhibited mitophagy. Since caspase 1 and caspase 11 have related functions, we also investigated them. We discovered common functions with regards to the LPS/IFNγ-mediated mitophagy inhibition. First, we found that both *caspase 1* and *11* are STAT1 target genes. Whereas STAT1-dependent regulation of *caspase 1* was unknown, the levels of *caspase 11* levels were previously shown to be upregulated by IFNγ but without demonstration of STAT1 involvement (39). Additionally, similarly to caspase 1, we showed that caspase 11 translocates to mitochondria upon LPS/IFNγ-mediated macrophage activation. More interestingly, using recombinant proteins, we showed that both caspase 1 and 11 were able to degrade PINK1. A similar property was previously depicted for caspase 11 towards TRPC1 (42). Besides this action, caspase 11 was shown to act as an intracellular sensor binding LPS (46, 47). Interestingly, the presence of LPS markedly increased the propensity of caspase 11 for degrading PINK1. Unexpectedly, we made similar observation for caspase 1. This further strengthens the

hypothesis of coordinated action of these two inflammatory caspases to block mitophagy by degrading PINK1 upon STAT1 activation and the presence of LPS intracellularly.

We studied the scope of this in vitro findings in vivo in murine models of polymicrobial infection (CLP) and endotoxemia (LPS injection). We showed with pharmacological modulators of mitophagy, as well as with transplantation of *Pink1*-deficient bone marrow, that the inhibition of mitophagy in myeloid cells leads to their activation, contributes to the reduction of bacterial infection and is associated with a better survival. These data also raise preliminary evidences of a potential therapeutic interest of pharmacological targeting of mitophagy in myeloid cells of septic patients. As we showed that the early measurement of mitochondrial density in blood monocytes by flow cytometry upon the onset of sepsis is a reliable marker of mitophagy level; this parameter was assessed in critically ill patients hospitalized in ICU with or without sepsis. Interestingly, we observed that mitochondrial density in blood monocytes (marker of mitophagy inhibition) was significantly increased in septic patients as compared to non-septic patients. Similarly to blood procalcitonin, a biomarker of severe infection classically used in the diagnosis of sepsis, mitochondrial density in blood monocytes was significantly correlated with blood level of C-reactive protein and only with this parameter among twenty blood biomarkers (inflammation, organ-dysfunction, tissue perfusion, hemodynamic). Therefore, we propose mitophagy level in blood monocytes as a biomarker of sepsis. Future studies will be required to investigate the level of mitophagy in blood monocytes according to sepsis severity, survival as well as type of infection in order to evaluate whether this parameter could be helpful in personalized patient care. Regarding the type of infection, our in vitro and in vivo findings in mice showed that the inhibition of mitophagy in myeloid cells is a feature of LPS and gram-negative infections. Among the set of critically ill patients studied, sepsis was not likely related to gram-negative infection in all cases. Nevertheless, the contribution of LPS in the inhibition of mitophagy in blood monocytes of critically ill patients cannot be excluded as our group recently showed, using a new high sensitive mass spectrometry method, that the blood levels of LPS are significantly higher in septic *vs* non-septic

patients whatever the type of infection (67). This phenomenon is likely due to the translocation of gram-negative bacteria because of the alteration of barrier functions in septic patients without regards of the primary infection. This will have to be studied with respect to mitophagy level in blood monocytes of critically ill patients. Finally, this work raises the hypothesis of the use of pharmacological modulators of mitophagy in septic patients. This strategy may enhance host defense and reverse sepsis-induced immuno-paralysis. Additionally, our data suggest that therapeutics endowed with mitophagy-modulating properties should be investigated in the context of septic patients. Such investigations should, in particular, explore the impact of antibiotics as recent studies highlighted important consequences of several classes of antibiotics on mitochondrial function (68). This may help understanding some unexplained therapeutic failure with certain antibiotics.

Methods

Reagents and antibodies.

See supplementary information.

Bacterial load

Peritoneal fluids and liver homogenates were subjected to serial 10-fold dilutions and cultured on 5% sheep blood agar (Oxoid) plates. Colony-forming units (CFUs) were quantified after 24h of incubation at 37°C in anaerobic conditions.

Recombinant protein assay

Recombinant proteins were stored à -80°C until used in PBS containing 15% glycerol. Recombinant T. Castaneum PINK1 (260ng) was incubated at 37°C with recombinant human caspase 1 (1U) or caspase 4/11 (1U) for indicated duration in 50µL assay buffer (50mM Hepes pH7.2, 50mM NaCl, 0.1% CHAPS, 10mM EDTA, 5% Glycerol, 10mM DTT). Then, proteins were denaturated for 5min at 100°C in Laemmli buffer and loaded on 2,2,2-trichloroethanol (TCE) gel (mini protean TGX, stain-free, 4-20% from Biorad). Proteins were visualized by UV transillumination.

Cellular studies

Raw 264.7 cells were obtained from ATCC (TIB-71) and cultured in RPMI 1640 medium containing L-glutamine supplemented with 10% FBS plus antibiotics (100 µg/ml penicillin, 100 µg/ml streptomycin). Murine bone marrow-derived macrophages (BMDMs) were generated from C57BL/6J mice and cultured in RPMI 1640 medium containing L-glutamine supplemented with 10% FBS, 20% L929-conditioned media plus antibiotics. Peritoneal macrophages were harvested from C57BL/6J mice by puncture of the peritoneal cavity after injection of 5mL of cold PBS 2mM EDTA (no thioglycollate elicitation). Peritoneal macrophages were allowed to attach for 12h (raw 264.7 cell medium). The medium was renewed after this period.

In vitro cell stimulation

See supplementary information.

Oxygen consumption rate (OCR) and Extracellular Acidification rate (ECAR)

Real-time OCR and ECAR in BMDMs were determined with a Seahorse XF96e Extracellular Flux Analyzer (Agilent Technologies). $4x10^4$ cells/well in 6-8 wells were used for each condition. The assay was performed in DMEM-based medium according to manufacturer's instructions. Four consecutive measurements were performed under basal conditions and three after the sequential addition of the following respiratory chain complex inhibitors (Mito Stress assay). OCR and ECAR data were normalized per µg of protein per well.

Cytokine quantification

Cytokines were measured, at the indicated time points, on cell culture media or mouse plasma according to manufacturer's instructions of luminex-based multiplex assays.

Macrophage activation

Cells were suspended in PBS 2mM EDTA. Fcγ Receptors were saturated with FcR blocking reagent according to manufacturer's instructions. After a washing step, cells were stained with anti-mouse CD64-APC, anti-mouse CD80-PE or anti-mouse CD86-PE antibodies according to the manufacturer's instruction (Miltenyi Biotec). Cells were maintained on ice until flow cytometry analysis.

Mitochondrial density

For in vitro studies, after stimulation, cells were incubated for 20min at 37°C in a humidified CO_2 incubator with pre-heated PBS containing 200nM mitotracker green FM. Cells were rinsed and resuspended in PBS 2mM EDTA. Cells were maintained on ice until flow cytometry analysis. For in vivo studies, hemolysis was performed on freshly collected blood samples or leukocytes obtained from peritoneal fluid. After rinsing, cells were incubated with PBS containing 200nM mitotracker green FM for 20min and saturated with FcR blocking reagent according to manufacturer's instructions. After a washing step, cells were stained with anti-mouse CD45-Viogreen; CD115-PE; Ly6G-VioBlue; Ly6C-APC; CD64-APC; CD80-PE; CD86-PE; F4/80-PerCP-Vio700; CD11b-APC-Vio770. Flow cytometry analysis was performed with a BD LSR II

Cytometer. For human studies, a similar procedure was used. After hemolysis and rinsing, cells were incubated with PBS containing 200nM mitotracker green FM for 20min. After a washing step, cells were placed on ice and stained with anti-human CD33-PE-Vio770, CD16-BV 421, anti-human CD14-BV 605), CD66b-APC-Vio770. Flow cytometry analysis was performed with a BD FACS Canto Cytometer.

Mitochondrial ROS production and Mitochondrial membrane potential

After stimulation, cells were incubated for 20 min at 37°C in a humidified CO_2 incubator with pre-heated PBS containing 2.5µM mitosox red (mROS) or 5µM JC-1 or 50nM TMRM (mitochondrial membrane potential). Cells were rinsed, re-suspended in PBS 2mM EDTA and analysezed by flow cytometry.

Flow cytometry assessment of Autophagy and Mitophagy

After stimulation, cells were stained with cyto-ID autophagy detection kit according to the manufacturer's instructions. Flow cytometry analysis was performed with a BD LSR II Cytometer. For flow cytometry assessment of mitophagy, raw 264.7 cells were transfected with mitochondial mKeima (mt-mKeima) expression vector or empty vector using JetPEI macrophages according to manufacturer's intructions. 24h after the transfection, the medium was changed and cells were exposed to LPS/IFNγ or vehicle for 6h or 24h. The spectral shift of mitochondrial-targeted mKeima (mt-mKeima) was assessed by flow cytometry using a BD LSRII Flow cytometer. During mitophagy, mKeima-expressed in mitochondria that are engulfed into lysosomes are excited at 561nm due to low lysosomal pH. In mitochondria that are not committed to mitophagy, mKeima is maintained in a neutral pH environment and emits a signal when excited at 406nm (69).

Gentamycin Protection assay

Raw 264.7 macrophages were exposed to 3-MA, 2,4-DNP or CCCP only prior to gentamycin protection assay. *E. coli*-GFP were added at a multiplicity of infection (MOI) of 10 into the medium of raw 264.7 cells and incubated for 1h at 37°C. Medium was then refreshed with medium

containing gentamycin in order to eliminate non phagocytized *E. coli*-GFP. Phagocytosis and intracellular lysis *E. coli*-GFP were followed by flow cytometry (see supplementary information).

Phagocytosis assays

Cells were stimulated and incubated at 37 °C with carboxylate-modified polystyrene, fluorescent red latex beads (~2-µm diameter) at a ratio of 50 beads/cell in the culture medium. After the 18h incubation, cells were washed with ice-cold PBS and analyzed by flow cytometry.

Flow cytometry analysis.

Unless specified, flow cytometry was performed with a BD LSR II flow cytometer. All flow cytometry data were then analyzed with FlowJo V10 software.

Mitochondria isolation

Mitochondria were isolated with a mitochondria isolation kit (Miltenyi Biotec) using anti-Tom22 antibodies coupled with magnetic microbeads, according to manufacturer's instructions.

Western blot analysis

See supplementary information.

Microscopy

For JC-1 and mitotracker green staining and cells transfected with pMito-LSSmOrange or empty vector, cells were plated on glass coverslips. After stimulation, glass coverslips were mounted in cold PBS and directly visualized with Axio imager 2 (Carl Zeiss Microscopy GmbH). For immunostaining, cells were frown on Labtek slides. After stimulation, cells were fixed with 4% paraformaldehyde by incubating for 10 minutes at 4°C. Cells were then permeabilized by incubating with PBS containing 0.1% Triton X-100. Blocking was carried out with PBST (PBS + 0.1% Tween 20) supplemented with 1% BSA and 10% Goat serum at 4°C for 30 min. Cells were then incubated with primary at 4°C overnight in a humidified chamber. Cells were then washed and incubated with specific secondary antibody conjugated with a fluorophore for 1 hour under humidified chamber in the dark. Preparations were visualized with a Leica SP2 confocal miscroscope. Images were analyzed with Image J software.

Quantitative PCR

See supplementary information.

Oxygen consumption

After stimulation, 4 x 10^6 cells were re-suspended in 1mL of pre-heated PBS at 37°C. Oxygen consumption was measured with Clark's electrodes.

Respiratory chain complex activity

Cells pellets were homogenized, and enzyme activities were measured by spectrophotometric methods as previously described (70).

Mouse studies

C57BL/6 mice were obtained from Charles River (France). *Pink1*$^{-/-}$ mice and control littermates were obtained from the Jackson Laboratory (USA). Animals were housed in a temperature- and humidity-controlled facility and fed a standard chow diet. Experiments were performed with age-matched female mice (8-12 weeks old). Cecal ligation and puncture (CLP) surgery was carried out as previously described (71). Blood sampling was performed by a retroorbital puncture in mice anaesthetized with isoflurane. Peritoneal washing was performed after euthanasia. 5mL of 2mM EDTA PBS were injected intraperitoneally and recovered by peritoneal puncture. Endotoxemia was induced by intraperitoneal injection of LPS (*E. coli* serotype O55:B5) administered at 0.5 or 15mg.kg^{-1} for 24h. 2,4-dinitrophenol was prepared in PBS and given by intraperitoneal injection (10 mg.kg^{-1}, single dose) 24h prior sham or CLP-surgery or LPS injection. In vivo toxicity of 2,4-DNP was extensively documented, with a LD_{50} of 72mg/kg reported in mice (72). Mdivi-1 (Bio-Techne) was diluted in sterile saline (1% DMSO) and gently sonicated before IP injection (50mg/Kg) to obtain a homogenous suspension. Control mice received vehicle only (5mL/kg, PBS plus 1% DMSO).

Bone marrow transplantation (BMT) 8 week-old female C57BL6/J recipient mice were irradiated with 11 Gy to trigger full medullary aplasia before transplantation. Suspension of bone marrow cells were prepared from femurs of 6 week-old male *Pink1*$^{+/+}$ or *Pink1*$^{-/-}$ mice. Recipient

mouse was injected with about 2×10^6 bone marrow cells through the tail vein. C57BL6/J recipient mice were given water containing enrofloxacin 5mg/kg for 2 weeks after transplantation. CLP was performed on chimeric mice after five weeks of recovery after BMT.

Human studies.

Critically ill patients aged ≥ 18 years admitted to the intensive care unit (ICU) of Dijon university hospital receiving at least one life support therapy for organ failure (e.g. mechanical ventilation, vasopressors or inotropic agents, renal replacement therapy, high flow nasal cannula) with or without sepsis were eligible for inclusion (observational study “Myelochondria”). Baseline severity of illness was assessed using the Simplified Acute Physiology Score (SAPS II), and the degree of baseline organ dysfunction was quantified using the Sequential Organ Failure Assessment (SOFA) score. Patients were prospectively classified into subgroups according to the sepsis-3 definition (53). Only blood samples collected on EDTA-coated tubes for routine hematology analysis (< 8 hours since admission in ICU) were used for flow cytometry analysis of mitochondrial density in blood monocytes. Biological parameters obtained within a similar timeframe were recovered from the medical records.

Statistical analysis

Statistical differences were analyzed with GraphPad Prism 8. Comparisons of two groups were calculated with unpaired Student's *t*-test with Welch’s correction. For comparisons with more than two groups, Brown-Forsythe and Welch ANOVA tests method were used. Correction for multiple comparisons was performed with the two-stage set-up method of Benjamini, Krieger and Yekutieli. For survival experiments, statistical significance was tested by Gehan-Breslow-Wilcoxon test. Correlations were analyzed with Spearman’s rank correlation. A *P* value of less than 0.05 was considered statistically significant. Results are presented as mean ± s.e.m with the exception of human studies for which the median is presented. All experimental values were obtained from the measurement of distinct samples and non-repeated measures of the same sample. Experiments were repeated at least two times with the exception of CLP experiment and

intraperitoneal LPS injection experiments in order to reduce the number of animals used according to the 3R rules and the requirements of the institutional animal care and use committee of the Université de Bourgogne-Franche-Comté. For microscopy and western blotting experiments, representative data are presented in the Figures.

Study Approval.

All studies with mice were conducted in accordance with the local guidelines for animal experimentation. Protocol no. 2512 and APAFIS#22339-2019100909387172v2 were approved by the institutional animal care and use committee of the Université de Bourgogne-Franche-Comté. All procedures performed in studies involving human participants were in accordance with the ethical standards of the institutional research committee (comité de protection des personnes (CPP), reference number 2013-A00095-40) and with the 1964 Helsinki declaration and its later amendments. All enrolled patients and/or their next of kin were informed and consent authorizing the use of biological samples was documented in the medical records of the patients by the investigator. The observational study “Myelochondria” is registered under the ClinicalTrials.gov identifier NCT04439617.

General methods statements.

No samples, mice, or studies were removed from the analyses with the exception of unexpected premature death during CLP or intraperitoneal LPS injection experiments. Experiments were not blinded and samples were not randomized in this study. Tissue culture samples were evaluated for mycoplasma contamination.

Author contributions: CT conceived, supervised experiments, analyzed the data and wrote the manuscript; LL supervised experiments, wrote the manuscript and secured funding; DP conceived and performed experiments, analyzed the data; AD and JPQ supervised human studies; MNg, JG, JB, VD, AR, MN, MR, DM, JA provided scientific expertise and critical reading of the manuscript; KVD, FM, VD, AD, AR, AJ, TB, TG, CM, NLG, SM, JB, FD, CS, NG performed experiments.

Competing interests: none**.**

Acknowledgements: The authors acknowledge A. Hamman, S. Monier, N. Pernet (Flow Cytometry Facility); C. Arnould, B. Gasquet (Microscopy and Histology Facilities), E. Charron, H. Choubley, V. Bergas, JP Pais De Barros (Lipidomic Facility); V. Saint-Giorgio (Animal Facility), J. Laurent (UMR PAM) for expert technical expertise. **Funding:** This work was supported by the INSERM (Centre de Recherche UMR 1231), the UBFC, the ANR Investissements d'Avenir Grant (ANR-11 LABX-0021, Labex Lipstic), the FEDER, and the Regional Council of Bourgogne Franche-Comte and the Ecole Polytechnique Fédérale de Lausanne (EPFL). DP was supported by a fellowship funded by the HEC Pakistan.

References

1. Angus DC, and van der Poll T. Severe Sepsis and Septic Shock. *New England Journal of Medicine.* 2013;369(9):840-51.
2. Nathan C. Points of control in inflammation. *Nature.* 2002;420(6917):846-52.
3. Cavaillon J-M, Eisen D, and Annane D. Is boosting the immune system in sepsis appropriate? *Critical Care.* 2014;18(2):216.
4. Murray PJ, Allen JE, Biswas SK, Fisher EA, Gilroy DW, Goerdt S, et al. Macrophage activation and polarization: nomenclature and experimental guidelines. *Immunity.* 2014;41(1):14-20.
5. Hotchkiss RS, Monneret G, and Payen D. Sepsis-induced immunosuppression: from cellular dysfunctions to immunotherapy. *Nature Reviews Immunology.* 2013;13(12):862-74.
6. Buck MD, Sowell RT, Kaech SM, and Pearce EL. Metabolic Instruction of Immunity. *Cell.* 2017;169(4):570-86.
7. O'Neill LAJ, Kishton RJ, and Rathmell J. A guide to immunometabolism for immunologists. *Nature Reviews Immunology.* 2016;16(9):553-65.
8. Mills EL, Kelly B, Logan A, Costa ASH, Varma M, Bryant CE, et al. Succinate Dehydrogenase Supports Metabolic Repurposing of Mitochondria to Drive Inflammatory Macrophages. *Cell.* 2016;167(2):457-70.e13.
9. Carchman EH, Whelan S, Loughran P, Mollen K, Stratamirovic S, Shiva S, et al. Experimental sepsis-induced mitochondrial biogenesis is dependent on autophagy, TLR4, and TLR9 signaling in liver. *The FASEB Journal.* 2013;27(12):4703-11.
10. Rocheteau P, Chatre L, Briand D, Mebarki M, Jouvion G, Bardon J, et al. Sepsis induces long-term metabolic and mitochondrial muscle stem cell dysfunction amenable by mesenchymal stem cell therapy. *Nature Communications.* 2015;6:10145.
11. Bravo-San Pedro JM, Kroemer G, and Galluzzi L. Autophagy and Mitophagy in Cardiovascular Disease. *Circulation Research.* 2017;120(11):1812-24.
12. Cheng S-C, Scicluna BP, Arts RJW, Gresnigt MS, Lachmandas E, Giamarellos-Bourboulis EJ, et al. Broad defects in the energy metabolism of leukocytes underlie immunoparalysis in sepsis. *Nature Immunology.* 2016;17(4):406-13.
13. Kim M-J, Bae SH, Ryu J-C, Kwon Y, Oh J-H, Kwon J, et al. SESN2/sestrin2 suppresses sepsis by inducing mitophagy and inhibiting NLRP3 activation in macrophages. *Autophagy.* 2016;12(8):1272-91.
14. Zhou R, Yazdi AS, Menu P, and Tschopp J. A role for mitochondria in NLRP3 inflammasome activation. *Nature.* 2011;469(7329):221-5.
15. Nakahira K, Haspel JA, Rathinam VAK, Lee S-J, Dolinay T, Lam HC, et al. Autophagy proteins regulate innate immune responses by inhibiting the release of mitochondrial DNA mediated by the NALP3 inflammasome. *Nature Immunology.* 2011;12(3):222-30.
16. Arulkumaran N, Deutschman CS, Pinsky MR, Zuckerbraun B, Schumacker PT, Gomez H, et al. Mitochondrial Function in Sepsis. *SHOCK.* 2016;45(3):271-81.
17. Youle RJ, and Narendra DP. Mechanisms of mitophagy. *Nature reviews Molecular cell biology.* 2010;12(1):nrm3028.
18. Georgakopoulos ND, Wells G, and Campanella M. The pharmacological regulation of cellular mitophagy. *Nature Chemical Biology.* 2017;13(2):136-46.
19. Piquereau J, Godin R, Deschênes S, Bessi VL, Mofarrahi M, Hussain SNA, et al. Protective role of PARK2/Parkin in sepsis-induced cardiac contractile and mitochondrial dysfunction. *Autophagy.* 2013;9(11):1837-51.
20. Thomas KJ, McCoy MK, Blackinton J, Beilina A, van der Brug M, Sandebring A, et al. DJ-1 acts in parallel to the PINK1/parkin pathway to control mitochondrial function and autophagy. *Human Molecular Genetics.* 2011;20(1):40-50.

21. Xiong H, Wang D, Chen L, Choo YS, Ma H, Tang C, et al. Parkin, PINK1, and DJ-1 form a ubiquitin E3 ligase complex promoting unfolded protein degradation. 2009.
22. Amatullah H, Shan Y, Beauchamp BL, Gali PL, Gupta S, Maron-Gutierrez T, et al. DJ-1/PARK7 Impairs Bacterial Clearance in Sepsis. *American Journal of Respiratory and Critical Care Medicine.* 2017;195(7):889-905.
23. Nathan C, and Cunningham-Bussel A. Beyond oxidative stress: an immunologist's guide to reactive oxygen species. *Nature Reviews Immunology.* 2013;13(5):nri3423.
24. Weinberg Samuel E, Sena Laura A, and Chandel Navdeep S. Mitochondria in the Regulation of Innate and Adaptive Immunity. *Immunity.* 2015;42(3):406-17.
25. Garaude J, Acín-Pérez R, Martínez-Cano S, Enamorado M, Ugolini M, Nistal-Villán E, et al. Mitochondrial respiratory-chain adaptations in macrophages contribute to antibacterial host defense. *Nature Immunology.* 2016;17(9):1037-45.
26. West AP, Brodsky IE, Rahner C, Woo DK, Erdjument-Bromage H, Tempst P, et al. TLR signalling augments macrophage bactericidal activity through mitochondrial ROS. *Nature.* 2011;472(7344):476-80.
27. Geng J, Sun X, Wang P, Zhang S, Wang X, Wu H, et al. Kinases Mst1 and Mst2 positively regulate phagocytic induction of reactive oxygen species and bactericidal activity. *Nature Immunology.* 2015;16(11):1142-52.
28. Andreux PA, Houtkooper RH, and Auwerx J. Pharmacological approaches to restore mitochondrial function. *Nature Reviews Drug Discovery.* 2013;12(6):465-83.
29. Xu Y, Jagannath C, Liu X-D, Sharafkhaneh A, Kolodziejska KE, and Eissa NT. Toll-like receptor 4 is a sensor for autophagy associated with innate immunity. *Immunity.* 2007;27(1):135-44.
30. Dodson MW, and Guo M. Pink1, Parkin, DJ-1 and mitochondrial dysfunction in Parkinson's disease. *Curr Opin Neurobiol.* 2007;17(3):331-7.
31. Pickles S, Vigié P, and Youle RJ. Mitophagy and Quality Control Mechanisms in Mitochondrial Maintenance. *Current Biology.* 2018;28(4):R170-R85.
32. Lachmandas E, Boutens L, Ratter JM, Hijmans A, Hooiveld GJ, Joosten LAB, et al. Microbial stimulation of different Toll-like receptor signalling pathways induces diverse metabolic programmes in human monocytes. *Nature Microbiology.* 2016;2(3):1-10.
33. Gomes LC, Benedetto GD, and Scorrano L. During autophagy mitochondria elongate, are spared from degradation and sustain cell viability. *Nature Cell Biology.* 2011;13(5):589-98.
34. Khacho M, Tarabay M, Patten D, Khacho P, MacLaurin JG, Guadagno J, et al. Acidosis overrides oxygen deprivation to maintain mitochondrial function and cell survival. *Nature Communications.* 2014;5.
35. Merx MW, Liehn EA, Janssens U, Lütticken R, Schrader J, Hanrath P, et al. HMG-CoA Reductase Inhibitor Simvastatin Profoundly Improves Survival in a Murine Model of Sepsis. *Circulation.* 2004;109(21):2560-5.
36. Venet F, Lepape A, and Monneret G. Clinical review: flow cytometry perspectives in the ICU - from diagnosis of infection to monitoring of injury-induced immune dysfunctions. *Crit Care.* 2011;15(5):231.
37. Yu J, Nagasu H, Murakami T, Hoang H, Broderick L, Hoffman HM, et al. Inflammasome activation leads to Caspase-1–dependent mitochondrial damage and block of mitophagy. *Proc Natl Acad Sci U S A.* 2014;111(43):15514-9.
38. Kahns S, Kalai M, Jakobsen LD, Clark BFC, Vandenabeele P, and Jensen PH. Caspase-1 and Caspase-8 Cleave and Inactivate Cellular Parkin. *Journal of Biological Chemistry.* 2003;278(26):23376-80.
39. Chin YE, Kitagawa M, Kuida K, Flavell RA, and Fu XY. Activation of the STAT signaling pathway can cause expression of caspase 1 and apoptosis. *Molecular and Cellular Biology.* 1997;17(9):5328-37.

40. Man SM, and Kanneganti T-D. Converging roles of caspases in inflammasome activation, cell death and innate immunity. *Nature Reviews Immunology.* 2015;16(1):7-21.
41. Kayagaki N, Warming S, Lamkanfi M, Walle LV, Louie S, Dong J, et al. Non-canonical inflammasome activation targets caspase-11. *Nature.* 2011;479(7371):117-21.
42. Py Bénédicte F, Jin M, Desai Bimal N, Penumaka A, Zhu H, Kober M, et al. Caspase-11 Controls Interleukin-1β Release through Degradation of TRPC1. *Cell Reports.* 2014;6(6):1122-8.
43. Woodroof HI, Pogson JH, Begley M, Cantley LC, Deak M, Campbell DG, et al. Discovery of catalytically active orthologues of the Parkinson's disease kinase PINK1: analysis of substrate specificity and impact of mutations. *Open Biology.* 2011;1(3):110012-.
44. Kane LA, Lazarou M, Fogel AI, Li Y, Yamano K, Sarraf SA, et al. PINK1 phosphorylates ubiquitin to activate Parkin E3 ubiquitin ligase activity. *The Journal of Cell Biology.* 2014;205(2):143-53.
45. Wauer T, Simicek M, Schubert A, and Komander D. Mechanism of phospho-ubiquitin-induced PARKIN activation. *Nature.* 2015;524(7565):370-4.
46. Hagar JA, Powell DA, Aachoui Y, Ernst RK, and Miao EA. Cytoplasmic LPS Activates Caspase-11: Implications in TLR4-Independent Endotoxic Shock. *Science.* 2013;341(6151):1250-3.
47. Shi J, Zhao Y, Wang Y, Gao W, Ding J, Li P, et al. Inflammatory caspases are innate immune receptors for intracellular LPS. *Nature.* 2014.
48. Chandel NS, McClintock DS, Feliciano CE, Wood TM, Melendez JA, Rodriguez AM, et al. Reactive Oxygen Species Generated at Mitochondrial Complex III Stabilize Hypoxia-inducible Factor-1α during Hypoxia: A MECHANISM OF O ₂ SENSING. *Journal of Biological Chemistry.* 2000;275(33):25130-8.
49. Shalova Irina N, Lim Jyue Y, Chittezhath M, Zinkernagel Annelies S, Beasley F, Hernández-Jiménez E, et al. Human Monocytes Undergo Functional Re-programming during Sepsis Mediated by Hypoxia-Inducible Factor-1α. *Immunity.* 2015;42(3):484-98.
50. Cheng SC, Quintin J, Cramer RA, Shepardson KM, Saeed S, Kumar V, et al. mTOR- and HIF-1 -mediated aerobic glycolysis as metabolic basis for trained immunity. *Science.* 2014;345(6204):1250684-.
51. Tannahill GM, Curtis AM, Adamik J, Palsson-McDermott EM, McGettrick AF, Goel G, et al. Succinate is an inflammatory signal that induces IL-1β through HIF-1α. *Nature.* 2013;496(7444):238-42.
52. Kong D, Park EJ, Stephen AG, Calvani M, Cardellina JH, Monks A, et al. Echinomycin, a Small-Molecule Inhibitor of Hypoxia-Inducible Factor-1 DNA-Binding Activity. *Cancer Research.* 2005;65(19):9047-55.
53. Singer M, Deutschman CS, Seymour CW, Shankar-Hari M, Annane D, Bauer M, et al. The Third International Consensus Definitions for Sepsis and Septic Shock (Sepsis-3). *JAMA.* 2016;315(8):801.
54. Zhong Z, Umemura A, Sanchez-Lopez E, Liang S, Shalapour S, Wong J, et al. NF-κB Restricts Inflammasome Activation via Elimination of Damaged Mitochondria. *Cell.* 2016;164(5):896-910.
55. Rademann P, Weidinger A, Drechsler S, Meszaros A, Zipperle J, Jafarmadar M, et al. Mitochondria-Targeted Antioxidants SkQ1 and MitoTEMPO Failed to Exert a Long-Term Beneficial Effect in Murine Polymicrobial Sepsis. *Oxidative Medicine and Cellular Longevity.* 2017;2017:1-14.
56. Ghanta S, Tsoyi K, Liu X, Nakahira K, Ith B, Coronata AA, et al. Mesenchymal Stromal Cells Deficient in Autophagy Proteins Are Susceptible to Oxidative Injury and Mitochondrial Dysfunction. *American Journal of Respiratory Cell and Molecular Biology.* 2017;56(3):300-9.

57. Mannam P, Shinn AS, Srivastava A, Neamu RF, Walker WE, Bohanon M, et al. MKK3 regulates mitochondrial biogenesis and mitophagy in sepsis-induced lung injury. *American Journal of Physiology-Lung Cellular and Molecular Physiology.* 2014;306(7):L604-L19.
58. Rambold AS, and Pearce EL. Mitochondrial Dynamics at the Interface of Immune Cell Metabolism and Function. *Trends in Immunology.* 2018;39(1):6-18.
59. Liu W, Acin-Perez R, Geghman KD, Manfredi G, Lu B, and Li C. Pink1 regulates the oxidative phosphorylation machinery via mitochondrial fission. *Proceedings of the National Academy of Sciences.* 2011;108(31):12920-4.
60. Requejo-Aguilar R, Lopez-Fabuel I, Fernandez E, Martins LM, Almeida A, and Bolaños JP. PINK1 deficiency sustains cell proliferation by reprogramming glucose metabolism through HIF1. *Nature Communications.* 2014;5(1).
61. Yao Z, Gandhi S, Burchell VS, Plun-Favreau H, Wood NW, and Abramov AY. Cell metabolism affects selective vulnerability in PINK1-associated Parkinson's disease. *Journal of Cell Science.* 2011;124(24):4194-202.
62. Sica A, and Mantovani A. Macrophage plasticity and polarization: in vivo veritas. 2012.
63. Bourke LT, Knight RA, Latchman DS, Stephanou A, and McCormick J. Signal transducer and activator of transcription-1 localizes to the mitochondria and modulates mitophagy. *JAKSTAT.* 2013;2(4).
64. Pitroda SP, Wakim BT, Sood RF, Beveridge MG, Beckett MA, MacDermed DM, et al. STAT1-dependent expression of energy metabolic pathways links tumour growth and radioresistance to the Warburg effect. *BMC Medicine.* 2009;7(1).
65. Sisler JD, Morgan M, Raje V, Grande RC, Derecka M, Meier J, et al. The Signal Transducer and Activator of Transcription 1 (STAT1) Inhibits Mitochondrial Biogenesis in Liver and Fatty Acid Oxidation in Adipocytes. *PLoS One.* 2015;10(12).
66. Broz P, and Dixit VM. Inflammasomes: mechanism of assembly, regulation and signalling. *Nature Reviews Immunology.* 2016;16(7):407-20.
67. Dargent A, Pais De Barros J-P, Ksiazek E, Fournel I, Dusuel A, Rerole AL, et al. Improved quantification of plasma lipopolysaccharide (LPS) burden in sepsis using 3-hydroxy myristate (3HM): a cohort study. *Intensive Care Med.* 2019;45(11):1678-80.
68. Moullan N, Mouchiroud L, Wang X, Ryu D, Williams Evan G, Mottis A, et al. Tetracyclines Disturb Mitochondrial Function across Eukaryotic Models: A Call for Caution in Biomedical Research. *Cell Reports.* 2015;10(10):1681-91.
69. Katayama H, Kogure T, Mizushima N, Yoshimori T, and Miyawaki A. A Sensitive and Quantitative Technique for Detecting Autophagic Events Based on Lysosomal Delivery. *Chemistry & Biology.* 2011;18(8):1042-52.
70. Bastin J, Aubey F, Rotig A, Munnich A, and Djouadi F. Activation of peroxisome proliferator-activated receptor pathway stimulates the mitochondrial respiratory chain and can correct deficiencies in patients' cells lacking its components. *J Clin Endocrinol Metab.* 2008;93(4):1433-41.
71. Deckert V, Lemaire S, Ripoll P-J, de Barros J-PP, Labbé J, Borgne CC-L, et al. Recombinant human plasma phospholipid transfer protein (PLTP) to prevent bacterial growth and to treat sepsis. *Scientific Reports.* 2017;7(1).
72. De Felice FG, and Ferreira ST. Novel neuroprotective, neuritogenic and anti-amyloidogenic properties of 2,4-dinitrophenol: The gentle face of Janus. *IUBMB Life.* 2006;58(4):185-91.

Figure legends

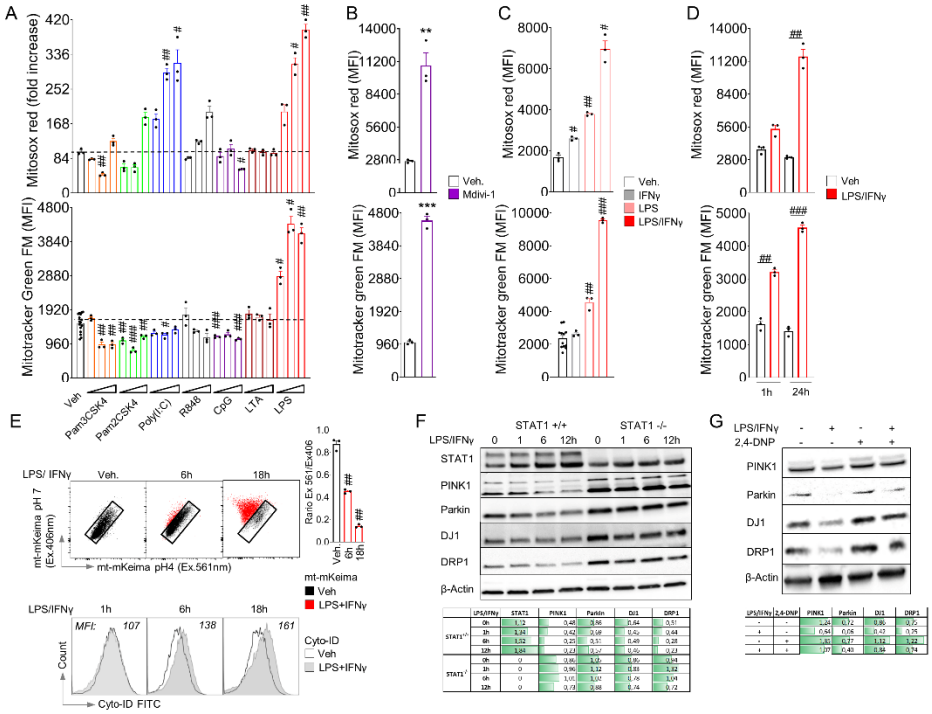

Figure 1. Macrophages activation is associated with the early inhibition of mitophagy
A-D. Flow cytometry assessment of mitochondrial ROS (upper panel) and mitochondrial density (lower panel) in raw 264.7 macrophages (**A**) exposed to TLR agonists, (**B**) mitophagy inhibitor (mdivi-1) or (**C-D**) to LPS and IFNγ alone in combination for 24h or specified duration (n=3 per condition). **E**. Flow cytometry assessment of mitophagy in raw 264.7 macrophages with mt-mkeima (upper panel) or autophagic vacuole formation with cyto-ID autophagy detection kit (lower panel) in raw 264.7 macrophages exposed to LPS/IFNγ. (n=3 per condition). **F-G**. Immunoblots of mitophagy and mitochondrial fission checkpoints on protein lysates from (**F**) *stat1*$^{+/+}$ or *stat1*$^{-/-}$ BMDMs exposed to LPS/IFNγ or (**G**) from raw 264.7 macrophages exposed for 24h to LPS/IFNγ alone or in combination with a mitophagy inducer (2,4-DNP, 1µM) (Densitometry: ratio to β-actin is presented above the immunoblots). Bar graphs represent mean ± s.e.m. with overlaid individual values; $^{\#}$ *P<0.05,* $^{\#\#}$ *P<0.01,* $^{\#\#\#}$ *P<0.001* determined by ANOVA corrected for multiple comparison; * *P<0.05,* *** *P<0.001* determined by *Student's t-test* with Welch's correction.

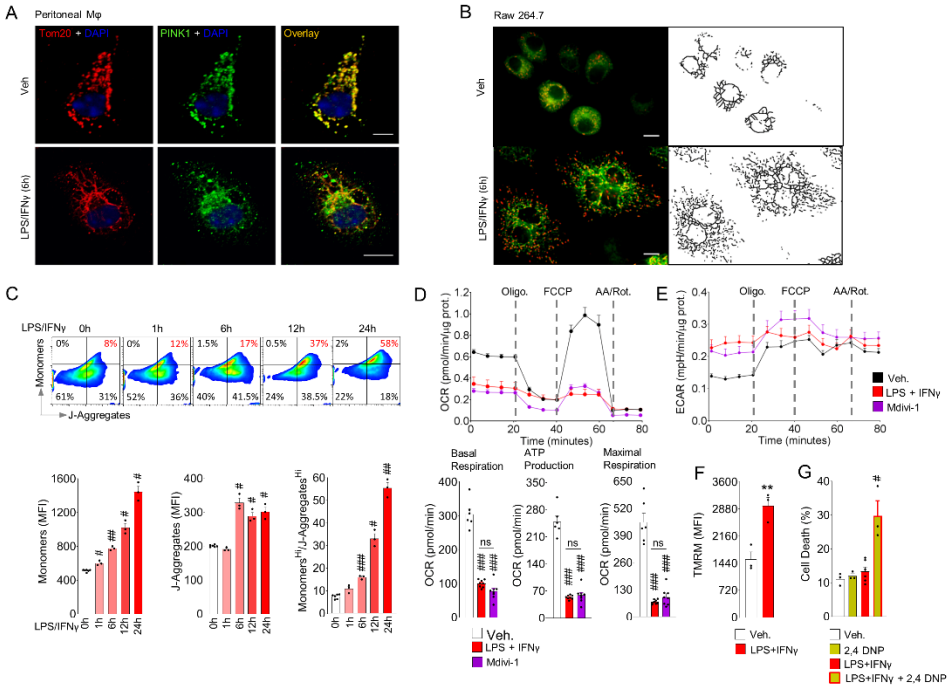

Figure 2. LPS/IFNγ-mediated inhibition of mitophagy is associated with metabolic reprogramming of macrophages.

A-B. Mitochondrial network of (**A**) mouse peritoneal macrophages or (**B**) raw 264.7 macrophages exposed to vehicle (veh) or LPS/IFNγ for 6h (**A**) immuno-stained for Tom20 in combination or not with PINK1 or (**B**) stained with JC-1 (right panels represent the image binarization of JC-1 stained macrophages). Scale bars: 10µm. **C**. Flow cytometry assessment of mitochondrial density and mitochondrial membrane potential in raw 264.7 macrophages exposed to LPS/IFNγ and stained with JC-1 (n=3 per time point). **D-E**. (**D**) Oxygen consumption (OCR) and extracellular acidification (ECAR) profile measured with Seahorse XFe96 analyzer on BMDMs exposed to vehicle (Veh.), LPS/IFNγ for 6h or Mdivi-1 for 24h (n=8 per condition). **F**. Flow cytometry assessment of mitochondrial membrane potential with TMRM in raw 264.7 macrophages exposed to LPS/IFNγ for 6h (n=3 per condition). **G**. Cell death assessed by low cytometry (annexin V - PI) in raw 264.7 macrophages exposed to vehicle (veh) or LPS/IFNγ and 2,4 DNP alone or combination for 18h. Bar graphs represent mean ± s.e.m. with overlaid individual values; $^{\#}$ *P<0.05,* $^{\#\#}$ *P<0.01,* $^{\#\#\#}$ *P<0.001* determined by ANOVA corrected for multiple comparison; ** *P<0.01*, *** *P<0.001* determined by *Student's t-test* with Welch's correction.

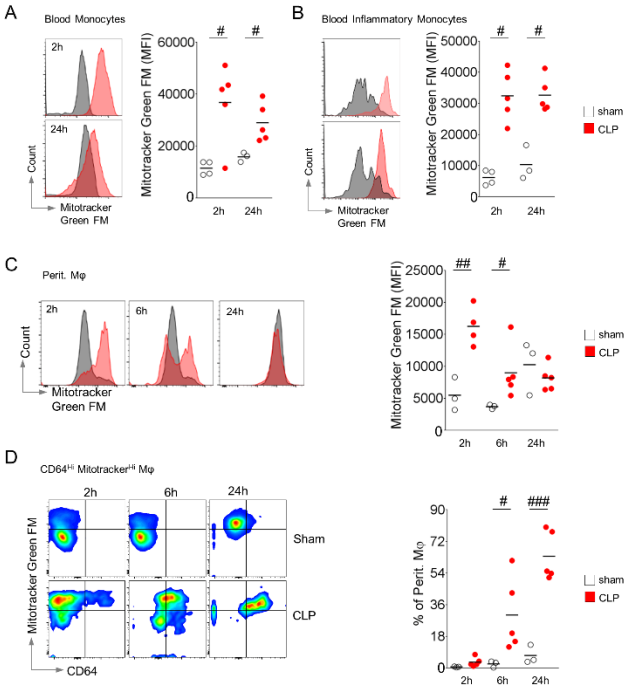

Figure 3. Polymicrobial infection triggers the early inhibition of mitophagy in myeloid cells. **A-B**. Flow cytometry assessment of the mitochondrial density in (**A**) total monocytes (CD45^{+} CD115^{+} CD11b^{Hi}) and in (**B**) inflammatory monocyte subpopulation (CD45^{+} CD115^{+} CD11b^{Hi} Ly6C^{Hi}) in the blood of C57BL6/J mice after sham- or cecal ligation and puncture (CLP) surgery (n=3-4 sham; n=5 CLP). **c**. Flow cytometry assessment of the mitochondrial density of peritoneal macrophages (CD45^{+} F4/80^{Hi} CD11b^{Hi}) in peritoneal fluid of mice operated as in **A-B**. **D**. Flow cytometry assessment of mitochondrial density in CD64^{Hi} Mitotracker^{Hi} subpopulation of peritoneal macrophages of mice operated as in **A-B**. Graphs with plots represent mean plus individual values; $^{\#}$ *P<0.05,* $^{\#\#}$ *P<0.01,* $^{\#\#\#}$ *P<0.001* determined by ANOVA corrected for multiple comparison.

Fig. 4

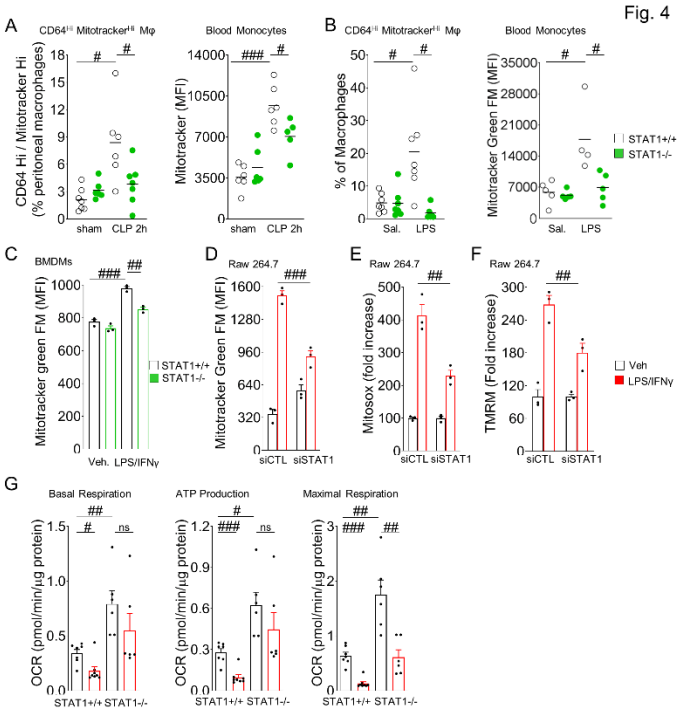

Figure 4. Polymicrobial infection and endotoxemia trigger the early inhibition of mitophagy in myeloid cells in a STAT1-dependent manner.

A-B. Flow cytometry assessment of CD64^{Hi} Mitotracker^{Hi} peritoneal macrophages subpopulation and mitochondrial density in blood monocytes of *stat1*$^{+/+}$ or *stat1*$^{-/-}$ mice after (**A**) sham- or cecal ligation and puncture (CLP) surgery (n= 6-7 sham; n=5.-7 CLP) or (**B**) intraperitoneal injection of saline (sal.) or LPS (0.5mg/kg, 24h) (n= 5-7 sal.; n=5-7 LPS). **C-D**. Flow cytometry assessment of mitochondrial density in (**C**) *stat1*$^{+/+}$ or *stat1*$^{-/-}$ BMDMs or in (**D**) raw 264.7 macrophages targeted with control (CTL) or stat1 siRNA then exposed to vehicle (veh.) or LPS/IFNγ for 24h. **E-F**. Flow cytometry assessment of (**E**) mitochondrial ROS production and (**F**) mitochondrial membrane potential in raw 264.7 macrophages targeted with control (CTL) or stat1 siRNA then exposed to vehicle (veh.) or LPS/IFNγ for 24h. **G**. Oxygen consumption profile measured with Seahorse XFe96 analyzer on *stat1*$^{+/+}$ or *stat1*$^{-/-}$ BMDMs exposed to vehicle (Veh.) or LPS/IFNγ for 6h (n=6-8 per condition).Graphs with plots represent mean plus individual values; Bar graphs represent mean ± s.e.m. with overlaid individual values; $^{\#}$ *P<0.05,* $^{\#\#}$ *P<0.01,* $^{\#\#\#}$ *P<0.001* determined by ANOVA corrected for multiple comparison.

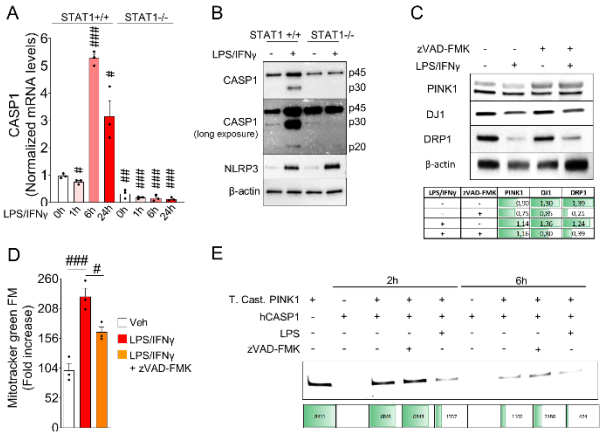

Figure 5. LPS/IFNγ inhibits mitophagy in macrophages through the STAT1-dependent regulation of caspase 1.

A-B. *Caspase 1* expression in *stat1*$^{+/+}$ or *stat1*$^{-/-}$ BMDMs exposed to vehicle or LPS/IFNγ for 18h or indicated duration assessed by (**A**) qPCR or (**B**) immunoblotting (n=3 per condition). **C-D**. Assessment by (**C**) immunoblotting or (**D**) flow cytometry of the impact of zVAD-FMK-dependent inhibition of caspases on LPS/IFNγ-dependent inhibition of mitophagy in raw 264.7 macrophages exposed to vehicle or LPS/IFNγ for 18h (n=3 per condition) (Densitometry: ratio to β-actin is presented above the immunoblots). **E**. Proteolytic activity of recombinant human caspase 1 (hCASP1) against recombinant Tribolium Castaneum PINK1 (T. Cast. PINK1) in the presence of zVAD-FMK and LPS (100ng/mL) alone or in combination. Protein levels were assessed with 2,2,2-trichloroethanol (TCE) gels after UV trans-illumination (table above presents densitometry data). Bar graphs represent mean ± s.e.m. with overlaid individual values; $^{\#}$ *P<0.05,* $^{\#\#}$ *P<0.01,* $^{\#\#\#}$ *P<0.001* determined by ANOVA corrected for multiple comparison.

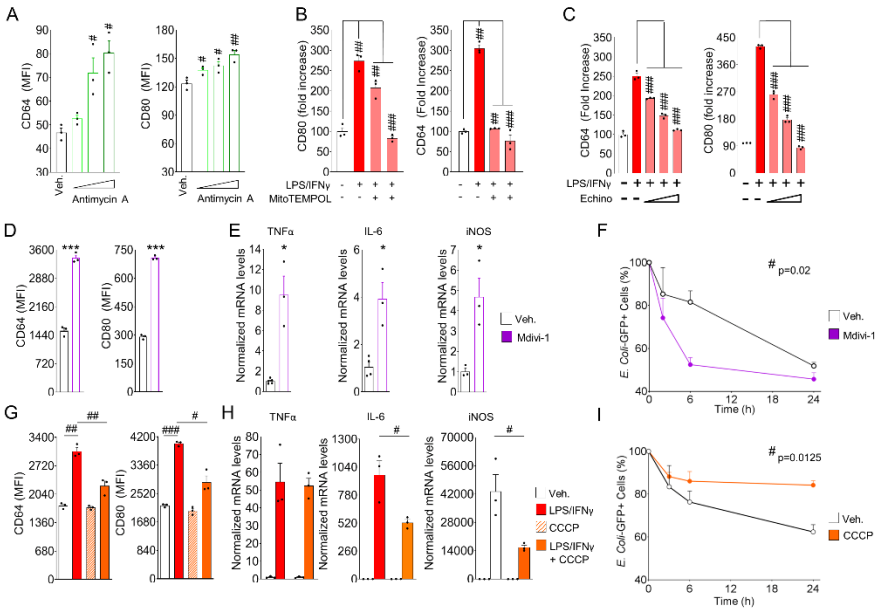

Figure 6. The inhibition of mitophagy triggers classical activation of macrophages through mitochondrial ROS.

A. Flow cytometry assessment of classical macrophage activation in raw 264.7 cells exposed to antimycin A for 6h. **B-C**. Flow cytometry assessment of classical macrophage activation in raw 264.7 cells exposed to LPS/IFNγ for 18h alone or in combination with (**B**) the mitochondrial ROS scavenger MitoTEMPOL or with (**C**) the HIF1α inhibitor echinomycin (n=3 per condition). **D-I**. Assessment of macrophage activation profile by (**D, G**) flow cytometry, (**E, H**) gene expression and (**F,I**) bactericidal activity in raw 264.7 cells (**D-E, G-H**) incubated (24h) or (**F, I**) pre-incubated (24h) with (**D-F**) the mitophagy inhibitor mdivi-1 or (**G-I**) the mitophagy inducer CCCP (n=3 per condition). Bar graphs represent mean ± s.e.m. with overlaid individual values; $^{\#}$ *P<0.05,* $^{\#\#}$ *P<0.01,* $^{\#\#\#}$ *P<0.001* determined by ANOVA corrected for multiple comparison; * *P<0.05,* *** *P<0.001* determined by *Student's t-test* with Welch's correction.

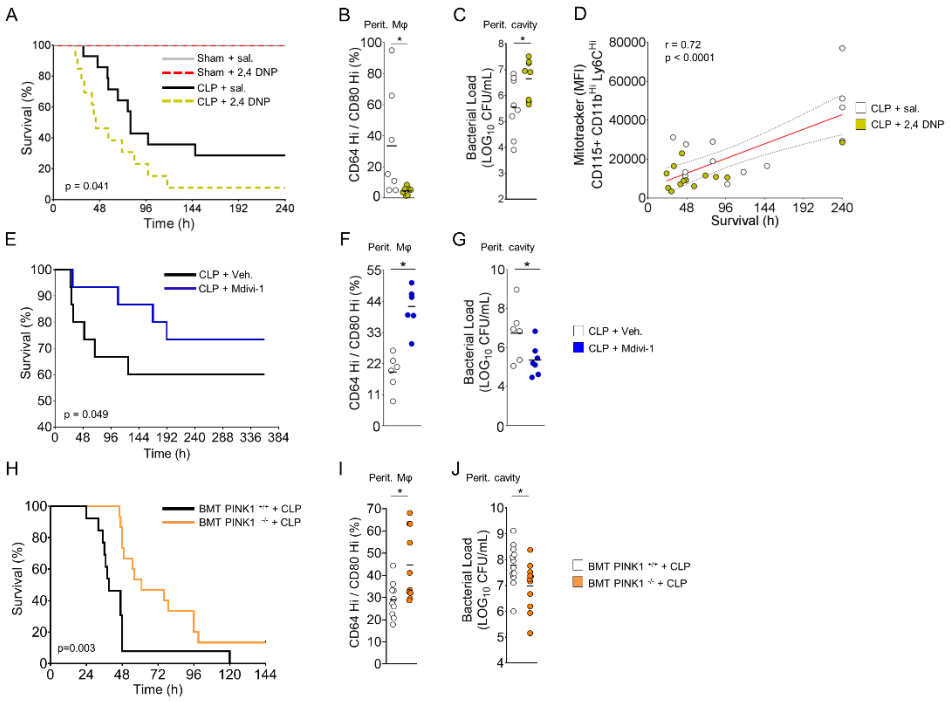

Figure 7. Inhibition of mitophagy in myeloid cells protects against bacterial infection and improves survival during sepsis.

A. Survival curve of C57BL6/J mice treated with saline (sal.) or 2,4-DNP (10mg/kg) 24h prior to sham- or cecal ligation and puncture (CLP) surgery (sham, n=5 per group; CLP, n=13 per group). *P value* was determined by *Gehan-Breslow-Wilcoxon test*. **B**. Percentage of classically activated macrophages (% of $CD11b^{Hi}$ $F4/80^{Hi}$ macrophages) in C57BL6/J mice treated as in **A** (n=7 per condition). **C**. Bacterial load in the peritoneal cavity of C57BL6/J mice treated as in **A** (n=8 per condition). **D**. Correlation of the mitochondrial density in $Ly6C^{Hi}$ blood monocytes 2h after CLP surgery versus the survival after CLP surgery (n=26). *r* and *p values* were determined by *Spearman's rank correlation*. **E**. Survival curve of C57BL6/J mice treated with vehicle or mdivi-1 for 24h prior to CLP surgery (CLP + Veh., n=15 ; CLP + mdivi-1, n=15). *P value* was determined by *Gehan-Breslow-Wilcoxon test*. **F-G**. Percentage of classically activated macrophages (**F**) (% of $CD11b^{Hi}$ $F4/80^{Hi}$ macrophages) and bacterial load (**G**) in the peritoneal cavity of C57BL6/J mice treated as in **e** (n=6-7 per condition) **H**. Survival curve of C57BL6/J mice transplanted with *Pink1*$^{+/+}$ (BMT *Pink1*$^{+/+}$) or *Pink1*$^{-/-}$ bone marrow (BMT *Pink1*$^{-/-}$) 5 weeks prior to CLP surgery (BMT *Pink1*$^{+/+}$, n=13; BMT *Pink1*$^{-/-}$, n=15). *P value* was determined by *Gehan-Breslow-Wilcoxon test*. **i.** Flow cytometry assessment the percentage of classically activated macrophages (% of $CD11b^{Hi}$ $F4/80^{Hi}$ macrophages) in the peritoneal cavity of mice which underwent transplantation and surgery as in **H** (n=11-12 per group). **J**. Bacterial load in the cavity of mice which underwent transplantation and surgery as in **H** (n=11-12 per group). Graphs with plots represent mean plus individual values; * *P<0.05* determined by *Student's t-test* with Welch's correction.

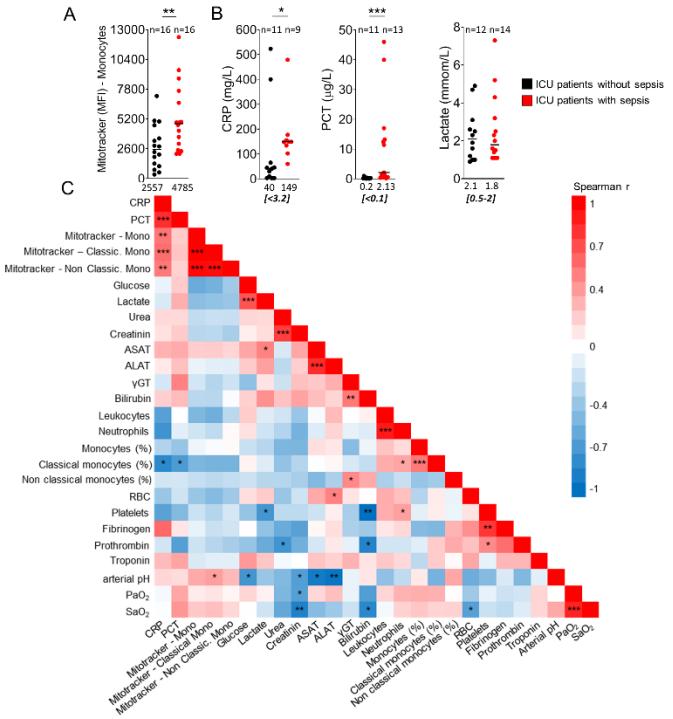

Figure 8. Increased mitochondrial density in blood monocytes is a biomarker of sepsis in critically ill patients.

A. Flow cytometry assessment of mitochondrial density in blood monocytes of critically ill patients (intensive care unit (ICU) patients) without (n=16) or with sepsis (n=16) according to sepsis-3 task force criteria. **B**. Levels inflammatory and tissue perfusion biomarkers in the blood of critically ill patients as described in **A**. Data were collected from patient medical record and were not available for all patients (n are indicated above graphs). Graphs represent median plus individual values. Median value of each group is presented at the bottom of each graph. Normal range of healthy patients are presented in bold italic enclosed in square brackets. * *P<0.05, ** P<0.01, *** P<0.001* determined by *Student's t-test* with Welch's correction. **C**. Correlation matrix of blood biomarkers in critically ill patients as described in **A** (n= 15-32). * *P<0.05, ** P<0.01, *** P<0.001* were determined by *Spearman's rank correlation*.